QUARTERLY JOURNAL OF THE ROYAL METEOROLOGICAL SOCIETY
Q. J. R. Meteorol. Soc. **136(s1)**: 174–189 (2010)
Published online 22 June 2009 in Wiley InterScience
(www.interscience.wiley.com) DOI: 10.1002/qj.439

Northward bursts of the West African monsoon leading to rainfall over the Hoggar Massif, Algeria

Juan Cuesta,[a,b]* Christophe Lavaysse,[b] Cyrille Flamant,[b] Mohamed Mimouni[c] and Peter Knippertz[d]

[a]*Laboratoire de Météorologie Dynamique/Institut Pierre Simon Laplace, École Polytechnique, Palaiseau, France*
[b]*Laboratoire Atmosphères, Milieux, Observations Spatiales/Institut Pierre Simon Laplace, Paris, France*
[c]*Office National de la Météorologie, Tamanrasset, Algeria*
[d]*Institut für Physik der Atmosphäre, Johannes Gutenberg Universität, Mainz, Germany*

ABSTRACT: The Hoggar Massif is a comparatively populated region in the Sahara, where water supply is a critical problem due to the lack of nearby sources and unaffordable water pumping. In the present paper, we analyse the influence of the West African monsoon (WAM) on precipitation over the Hoggar during summer. We investigate (1) two rainfall events during 23–27 July 2006, accounting for almost half of the precipitation of this year, and (2) the representativity of this period with regard to ERA-40 ECMWF re-analyses (1979 to 2001).

By the end of July 2006, two consecutive northward bursts of the WAM flow reached the Hoggar and caused an increase in low-level humidity. In the afternoon of these days, clouds formed at the top of the convective boundary layer and rapidly grew to more than ∼9 km above mean sea level. Due to the comparatively moist sub-cloud layer (>45% mean relative humidity), considerable amounts of precipitation could reach the ground. The strong southerly WAM flow one day before and during the arrival of the moist air over the Hoggar is associated with both a south sector of an African easterly wave (AEW) and the cyclonic circulation around the south-eastern flank of the Saharan heat low (SHL). In addition, the northward excursions of the monsoon were supported by convective cold-pool outflows originating over Niger. The climatological analysis confirms the relation between precipitation over the Hoggar and AEW south sectors and also shows a conspicuous weakening of the SHL following rainfall. Copyright © 2009 Royal Meteorological Society

KEY WORDS African easterly waves; Saharan heat low; Saharan dust; CloudSat; CALIPSO

Received 16 December 2008; Revised 10 April 2009; Accepted 24 April 2009

1. Introduction

Water supply is a crucial societal problem for most populated regions in the Sahara, being the main driver for health, food security and the economy. This issue is even more critical in elevated locations, far from natural sources as in the Hoggar Massif (Algeria). Tamanrasset is the biggest city in the region, located at 1370 m above mean sea level (msl) and at 22.8°N, 5.5°E (see Figure 1). Its population has been rapidly growing in the last decades, accounting nowadays for nearly 80 000 inhabitants. Water pumping is not affordable since the closest significant water source In Salah (27.2°N, 2.5°E) is located ∼1000 m below Tamanrasset's ground level and ∼600 km away. Water is mainly supplied by rare rainfall events (typically 5 to 6 days of precipitation in Tamanrasset from July to September) and some other expensive and generally insufficient solutions (i.e. long-distance road transportation, nearby small sources). Although clouds and sometimes virga† are commonly observed in Tamanrasset (e.g. Cuesta *et al*., 2008), the annual amount of precipitation (on average between 1979 and 2006) is only ∼60 mm in Tamanrasset (located on the Hoggar plateau) and ∼160 mm in Assekrem (23.3°N, 5.6°E, see Figure 1) at 2780 m msl (located near Mount Tahat, the highest peak in the Hoggar which reaches 2918 m msl). Besides important implications for precipitation, enhanced understanding of the mechanisms leading to the formation of deep convection clouds over the Hoggar will improve the quantification of their impact on Saharan climate and radiative budget at the regional scale.

Previous work (e.g. Dubief, 1963, 1979; Cuesta *et al*., 2008) has postulated a possible link between summer precipitation in the Hoggar and southerly moisture advection associated with the West African monsoon (WAM). This generally occurs in response to the large-scale pressure gradient between the Gulf of Guinea and the Sahara, when the Saharan heat low (SHL) is deepest and located west of the Hoggar (e.g. Lavaysse *et al*., 2009b). The leading edge of the WAM, generally referred to as the intertropical discontinuity (ITD, i.e. the near-surface boundary between the south-westerly moist monsoon and the north-easterly dry harmattan winds) reaches the Sahel in May (e.g. Bock *et al*., 2008; Couvreux *et al*., 2009;

*Correspondence to: Juan Cuesta, Laboratoire de Météorologie Dynamique/Institut P. S. Laplace, Ecole Polytechnique, 91128 Palaiseau, France. E-mail: cuesta@lmd.polytechnique.fr

†Wisps or streaks of water or ice particles falling out of a cloud but evaporating before reaching the earth's surface as precipitation.

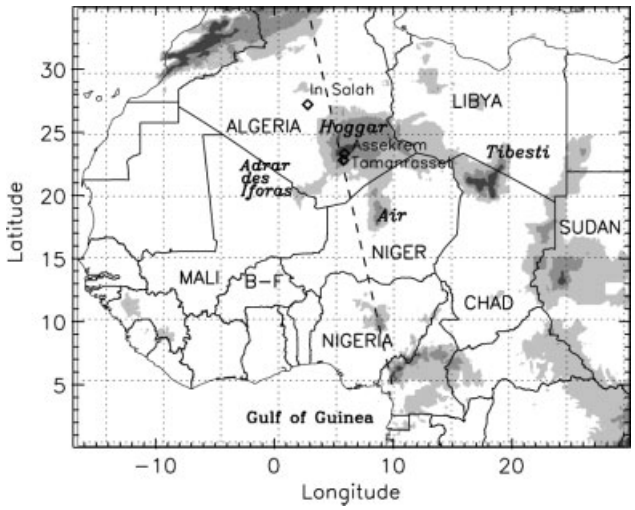

Figure 1. Map of North and West Africa with geographical labels (relevant orographic features appearing in italic). The grey shading indicates terrain height above mean sea level (m): 650, 1000 and 1500 m from light to dark grey. The dashed line represents CloudSat spaceborne radar track on 27 July 2006 at 1307 UTC. B-F denotes Burkina-Faso.

Guichard *et al*., 2009) and the southern fringes of the Sahara in late July and in August (Sultan and Janicot, 2000, 2003). During this period, strong low-level south-westerly winds occur along the south-eastern flank of the SHL which is located west of the Hoggar (Lavaysse *et al*., 2009b). As a result, the ITD often reaches its northernmost position as a northward prominence in the longitude band 0–5°E (just west of the Hoggar).

Furthermore, the passage of African easterly waves (AEWs) in the 15°–20°N latitudinal band (with a typical period of 3 to 5 days, best detected at 850 hPa) and/or modulations of the SHL strength (e.g. Couvreux *et al*., 2009; Lavaysse *et al*., 2009a) have the potential to either enhance or decrease the south-westerly low-level circulation, thereby modifying the position of the ITD at the synoptic time-scale. For instance, Fink and Reiner (2003) have shown that the increase of instability west of an AEW trough and the northward transport of humidity by the south sector of the wave provide favourable conditions for convection over the Sahel and the southern Sahara.

At daily time-scales, the position of the ITD is modulated by the diurnal cycle of the planetary boundary-layer (PBL) winds, its northernmost position being observed in response to the nocturnal low-level jet (Parker *et al*., 2005). Cold pools related to mesoscale convective systems (MCS) present over the Sahel during the summer may also contribute to the northward progression of the ITD (e.g. Flamant *et al*., 2009). Cool pools propagate rapidly over long distances and can lift up substantial amounts of dust (Knippertz *et al*., 2007; Marsham *et al*., 2008). Depending on the details of their generation and track, they carry moister or drier air than their surroundings (Miller *et al*., 2008; Flamant *et al*., 2009).

In the present paper, we analyse the influence of the WAM on rainfall over the Hoggar. To date, this link as well as the connection with the large-scale conditions has not been assessed, mostly due to the paucity of relevant observations in the Sahara. Improvement in the understanding of the WAM behaviour and the interactions with the main components of the West African climate (including the Sahara) has motivated a large international field campaign in West Africa during 2006 in the framework of the African Monsoon Multidisciplinary Analysis (AMMA: Redelsperger *et al*., 2006; Lebel *et al*., 2009). Within the AMMA project, the importance of the Saharan climate has long been recognised and has led to an ambitious experimental strategy which included the deployment of a suite of remote sensing instruments in Tamanrasset (Cuesta *et al*., 2008).

First, we present a detailed case-study of two rainfall events taking place from 23 to 27 July 2006 (leading to nearly half of the total annual precipitation in the Hoggar in 2006). It is worth noting that the total rainfall in Tamanrasset (59 mm) and in Assekrem (186 mm) in 2006 is representative of the average rainfall between 1979 and 2006. The meteorological conditions over the Hoggar prior to and during the precipitation events are described (in section 3). The impact on precipitating clouds of the increase in low-level moisture induced by the arrival of the WAM over the Hoggar is discussed. Then, particular attention is given to the contributions from different components of the WAM (namely the SHL, the AEWs and the MCS cold pools) leading to its northward burst over the Hoggar (section 4). The representativity of the event detailed in the case-study is assessed for the period from 1979 to 2001 (section 5). Conclusions are given in section 6.

2. Datasets

The local conditions prior to and during the rain events in the Hoggar are investigated using surface measurements of precipitation, humidity, temperature and dust number concentration performed at the stations of Tamanrasset and Assekrem, operated routinely by the Algerian Office National de la Météorologie (ONM). The vertical thermodynamic structure of the atmosphere over Tamanrasset is described using four daily radiosoundings (at 0000, 0600, 1200 and 1800 UTC). We use low-resolution data interpolated between the significant levels for each variable (available at http://weather.uwyo.edu/upperair/sounding.html). Complementary observations from a sun photometer and particle counters in Tamanrasset were available thanks to the deployment in 2006 of the French atmospheric mobile observatory MOBILIS (Moyens Mobiles de Télédétection de l'Institut Pierre Simon Laplace; see Cuesta *et al*., 2008) in the framework of AMMA.

The diurnal cycle and horizontal extent of clouds over or in the vicinity of the Hoggar are investigated using infrared satellite imagery from SEVIRI (Spinning Enhanced Visible and Infra Red Imager, with 15-minute temporal resolution) onboard MSG (Meteosat Second Generation) via false-colour images (available on http://aoc.amma-international.org/). The

propagation of MCS-related cold pools towards the western Hoggar is also tracked using SEVIRI false-colour images (http://loaamma.univ-lille1.fr/AMMA/). Cold-pool outflows offer an efficient mechanism for dust lifting due to the high winds and the turbulence existing near their leading edges (e.g. Flamant *et al*., 2007; Marsham *et al*., 2008). As a result the leading edge of a cold pool can be identified as an arc-shaped dust plume moving away from the parent MCS in the SEVIRI images.

The vertical extent of the precipitating clouds is analysed using measurements of the spaceborne radar CloudSat (Stephens *et al*., 2002) and spaceborne lidar onboard CALIPSO (Cloud-Aerosol Lidar and Infrared Pathfinder Satellite Observation; see Winker *et al*., 2007) satellite. They both have a narrow footprint (1.4 km for CloudSat and 0.09 km for CALIPSO lidar) and they are both aligned in the same so-called A-Train orbit, which follows a repetitive cycle of 16 days with four daytime overpasses over the Hoggar (from 1200 to 1400 UTC).

Large-scale conditions in West Africa leading to rainfall in the Hoggar are investigated using operational analyses of the European Centre for Medium-range Weather Forecasts (ECMWF) for 2006 (with a 0.5° resolution). For the climatological study, the satellite period of the ECMWF ERA-40 re-analysis data (with a 1.25° resolution) from 1979 to 2001 is used, generally regarded as the more reliable part of the dataset (Kållberg *et al*., 2005). The location and evolution of the SHL is determined by the relative maximum thickness between the geopotential heights at 700 hPa and 925 hPa (as in Lavaysse *et al*., 2009b). The SHL is defined as the region where the thickness between the geopotential heights exceeds 90% of its cumulative probability distribution over West Africa (Lavaysse *et al*., 2009b). The position of the ITD is identified by the minimum in geopotential at 925 hPa, indicating the location of the monsoon trough at the ITD (as in Lafore *et al*., 2007). Over the Hoggar (which is above the 925 hPa level and over which the previous criterion cannot be used), the movements of the ITD are tracked using a criterion based on the surface convergence between south-westerly and north-easterly winds at 10 m above ground level (Lafore *et al*., 2007). It is worth noting that ECMWF analyses can be used to track the ITD displacement resulting from its interaction with cold pools, provided that surface data relevant to its monitoring are assimilated (e.g. Flamant *et al*., 2009). Over the Sahara, the quality of the ECMWF analyses is likely to be worse due to the paucity of synoptic stations and radiosonde data (e.g. Knippertz *et al*., 2009). ECMWF analyses in this region are mainly dominated by model physics and assimilated satellite data. However, during the AMMA Special Observing Period (i.e. 2006) the increase of data assimilated over and south of the Sahel likely enhanced this capability through a better description of MCSs and related cold pools south of the Sahara.

The AEWs are detected using ECMWF 850 hPa wind fields at 0600 UTC (e.g. Fink and Reiner, 2003). Wind time series at each grid point are processed independently using a Butterworth band-pass numerical filter between 3 and 5 days. The AEW north (south) sectors are then identified from the spatial coherence of northerly (southerly) filtered winds stronger than a threshold of 0.5 m s^{-1}. The locations of troughs and ridges are determined by visual inspection of the filtered wind fields and also verified by 3–5-day filtered relative vorticity fields (e.g. Fink and Reiner, 2003).

3. Rainfall over the Hoggar from 23 to 27 July 2006

The rainfall in the Hoggar from 23 to 27 July 2006 corresponds to a typical summer rainy episode, accounting for 26.5 mm in Tamanrasset and 43 mm in Assekrem (in four days). These values correspond to 45% and 23% of the rainfall in 2006 in Tamanrasset and in Assekrem, respectively. In the following, we present a description of the prevailing meteorological conditions during the event (section 3.1) and the origin and characteristics of the precipitating clouds (section 3.2).

3.1. Local meteorological conditions

Rain-gauge observations show that precipitation occurs during the afternoon (after 1400 UTC) of 23, 24, 26 and 27 July both in Tamanrasset and in Assekrem (see Figure 2(a)). In Tamanrasset (1.4 km msl) and Assekrem (2.8 km msl), the precipitation (from rain gauges, Figure 2(a)) and the cloud cover (i.e. the horizontal fraction of the sky covered by clouds, estimated by an ONM operator, Figure 2(b)) exhibit a marked diurnal cycle. It rains every day, shortly after 1200 UTC, for ∼3 and ∼8 hours on average in Tamanrasset and in Assekrem, respectively. However, on 23 and 28 July, it rains more in Tamanrasset than in Assekrem. The cloud cover in Assekrem is generally observed to increase with time from a value of $\leqslant$25% at 0900 UTC and to reach 100% by 1500 UTC, except on 27 July. In Tamanrasset, a similar diurnal cycle is observed on 26 and 27 July only.

Figures 3(a) and 3(b) show the occurrence of two maxima of humidity in the convective boundary layer (CBL) during the days of precipitation between 23 and 28 July. In coincidence with the only rainfall events of the month, the relative humidity (RH) and water vapour mixing ratio (q) averaged in the CBL exceeded a threshold of ∼45% and ∼7 g kg^{-1}, respectively (see also Table I). ECMWF analyses in Figure 3(c) show that this increase is associated with the northward advance of the humidity front at the ITD. A Hovmüller diagram of q at 850 hPa (averaged between 2°E and 6°E) shows that the 7 g kg^{-1} contour shifts from ∼19°N to ∼23°N on the days when precipitation is observed in the Hoggar (Figure 3(c)). Figure 2(b) shows that cloud cover around mid-July (13th to 15th) in Tamanrasset (Assekrem) reaches values near 80% (90%) with a similar diurnal cycle, but without rain at the surface, probably due to too-low humidity in the CBL (RH <40% and $q < 6$ g kg^{-1}; see Figure 3(a)–(b)). On 25 July, this also occurs as humidity drops in between the rainy days (Figure 3(a)–(b), see Table I), due to the withdrawal of the WAM (Figure 3(c)).

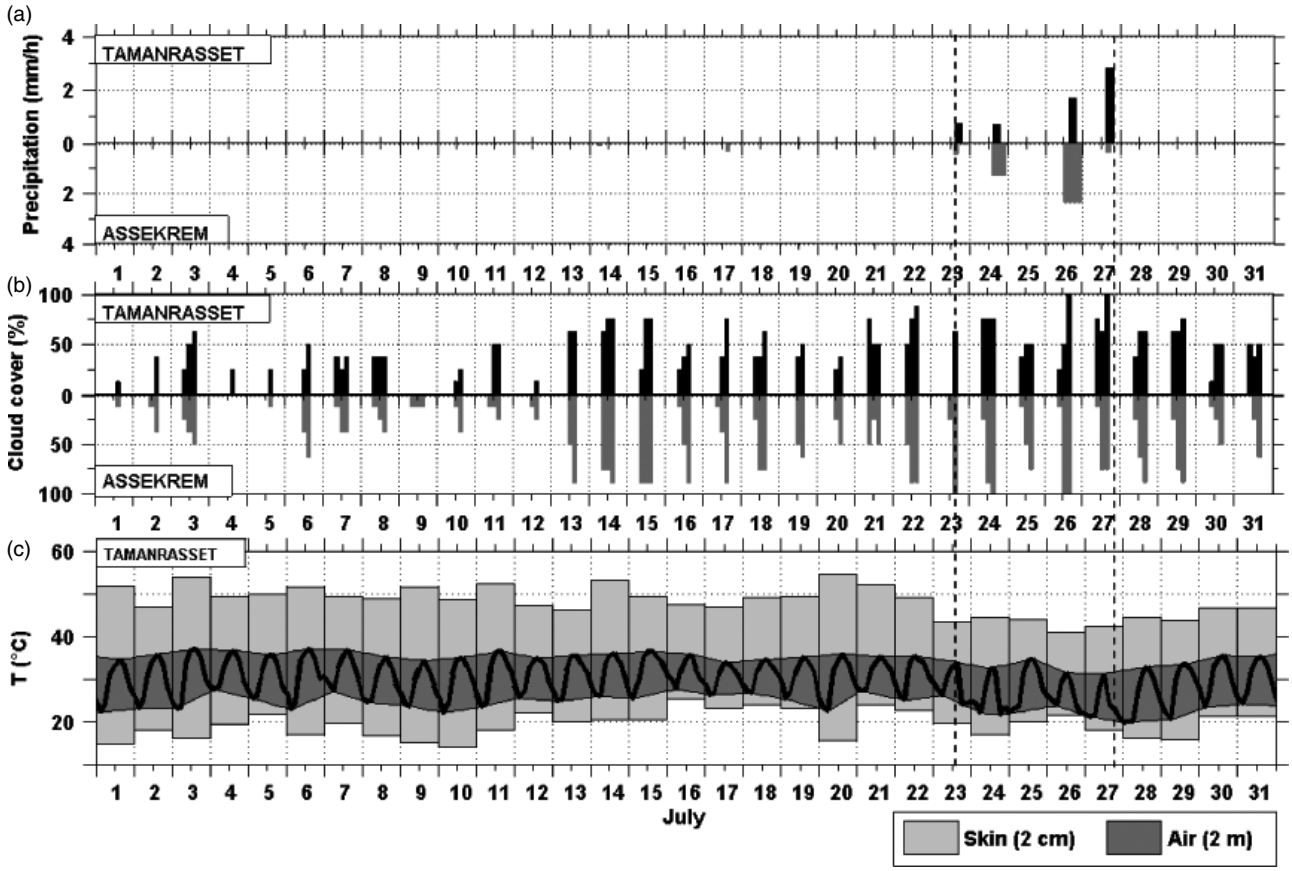

Figure 2. (a) Precipitation in Tamanrasset and Assekrem in July 2006 (amount in mm per hour and duration). (b) Fraction of the sky covered by clouds at 0900, 1200 and 1500 UTC at Tamanrasset and Assekrem. (c) Daily maximum and minimum temperature at 2 cm (skin, light grey) and at 2 m (air, in dark grey shade and every 3 hours in black line). Vertical dashed lines indicate the period of precipitation.

Table I. Atmospheric vertical structure from 23 to 27 July 2006, derived from Tamanrasset radiosondes at 1200 UTC. The CBL top altitude z_i is estimated as the lowest critical inversion according to Heffter (1980), using $\Delta\theta/\Delta z \geqslant 0.0025$ K m^{-1} and $\theta_{top} - \theta_{base} \approx 1$ K as criteria to account for the overshooting of thermals, as done by Cuesta *et al.* (2008).

Date	**CBL top** (km msl)	***RH* in the CBL** (%)	***q* in the CBL** (g kg^{-1})	**LCL** (km msl)	**LFC** (km msl)	**−20°C level** (km msl)
23 July	3.9	43	6.7	4.2	4.8	8.2
24 July	4.0	51	7.6	4.0	4.4	8.2
25 July	5.3	40	4.2	4.9	–	8.1
26 July	3.4	51	8.7	3.5	4.1	8.2
27 July	3.8	49	7.4	3.7	4.7	7.9

During the presence of the moist monsoonal air in Tamanrasset, the lifting condensation level (LCL) drops with respect to the previous days. During this period, the CBL top systematically reaches the LCL in the afternoon (Figure 3(b)), enabling condensation and thus formation of clouds. This is consistent with the diurnal evolution of cloud cover in Tamanrasset and Assekrem (Figure 2(b)) and over the Hoggar as observed using SEVIRI (Figure 4) during the days of precipitation. During the afternoons of the four days, the precipitating clouds are seen to form and grow over the Hoggar (see cloud cover within the red circles of Figure 4), and not to be advected or to propagate towards it. On 23 July, clouds start forming around midday, between 1200 and 1400 UTC, i.e. more than 3 h after the arrival of the moist WAM-related air mass. The onset of precipitation is at 1500 UTC in both Tamanrasset and Assekrem. However, it rained for a longer period in Tamanrasset than in Assekrem (according to rain-gauge observations). In the morning of 24 July, the trailing anvil clouds left over from deep convection on the previous day dissipate to the south-west of the Hoggar (Figure 4). Deep convection begins to develop over the Hoggar around 1200 UTC and strongly intensifies after 1400 UTC. Similar situations with residual clouds dissipating during the morning and local formation of precipitating clouds after midday are observed on 26 and 27 July (Figure 4).

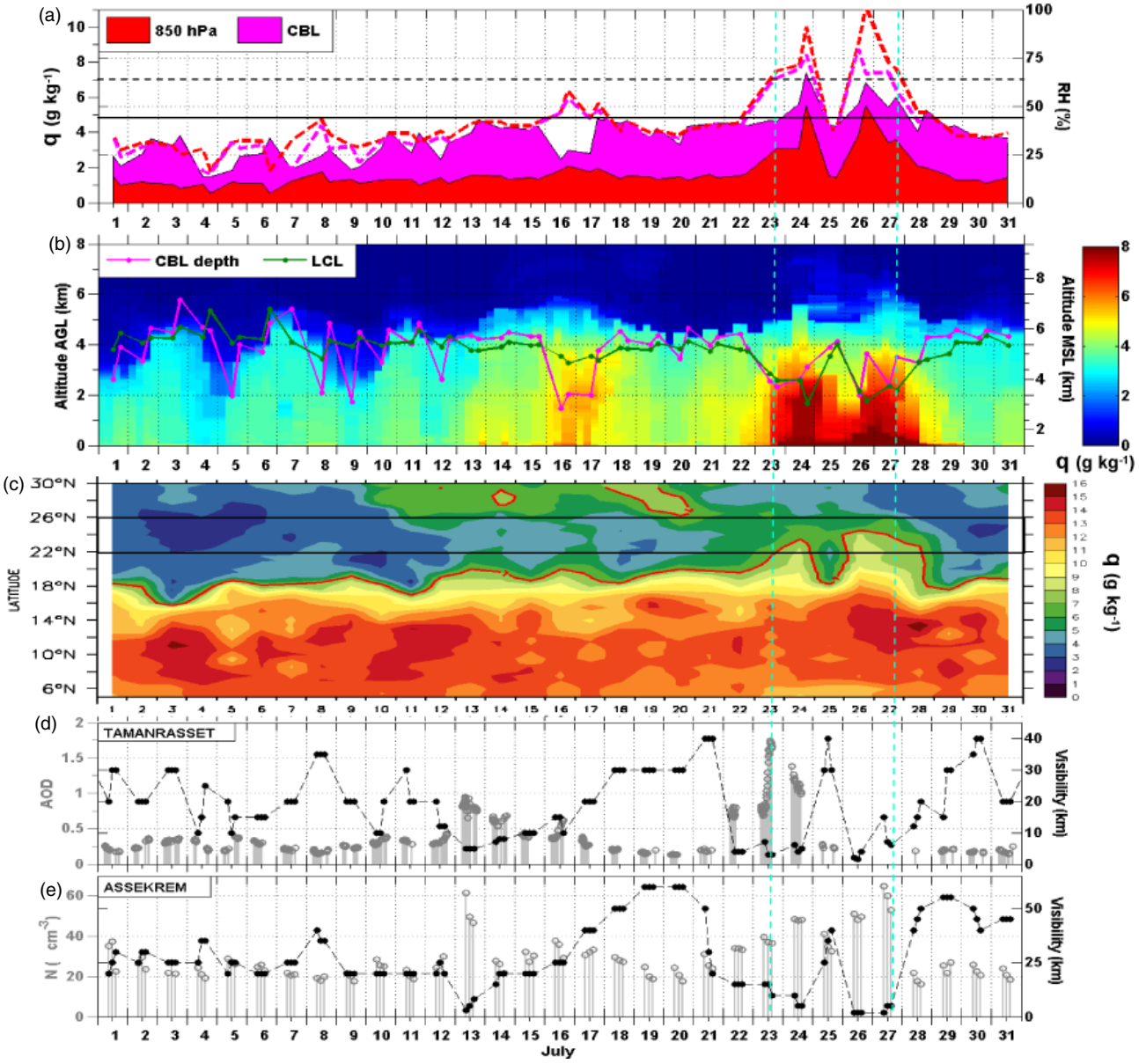

Figure 3. (a) Relative humidity *RH* (shade) and water vapour mixing ratio *q* (lines) in July 2006 from Tamanrasset radiosondes at 1200 and 1800 UTC, averaged over the CBL (light grey, pink) and at 850 hPa (dark grey, red). (b) Time series of *q* profiles over Tamanrasset, the CBL height at 1200 and 1800 UTC (light grey, pink) and the LCL (dark grey, green). (c) Latitude–time plot of *q* averaged between 2°E and 6°E from 850 hPa ECMWF analyses at 1200 UTC, the 7 g/kg iso-contour in grey (red) and black lines indicating the latitude of the Hoggar. (d) *AOD* (grey) from the MOBILIS sun photometer in Tamanrasset (available at http://aeronet.gsfc.nasa.gov/) and horizontal visibility (black) in Tamanrasset as estimated by an ONM operator. (e) Number concentration of particles with diameter from 0.3 to 5 μm at the surface (grey) and horizontal visibility (black) in Assekrem (ONM routine measurements). Vertical dashed lines indicate the period of precipitation. This figure is available in colour online at www.interscience.wiley.com/journal/qj

During the month of July 2006, surface temperature over the Hoggar only shows a significant decrease after the precipitation events (Figure 2(c)). As it starts raining on 23 July at 1500 UTC, air temperature (at 2 m above ground level (agl)) and surface temperature (at 2 cm agl) in Tamanrasset significantly drop by ∼7°C and ∼6°C, respectively (see Figure 2(c)). Air and surface temperatures over the Hoggar derived from ECMWF analyses (not shown) are broadly consistent with this behaviour. This suggests the absence of any particular influence of temperature in the Hoggar on water vapour condensation (e.g. increase in *RH*) and/or on atmospheric circulation (e.g. mountain–valley breeze), prior to the rainfall events. This implies that the only limiting factor for precipitation over the Hoggar is low-level moisture.

3.2. Formation and vertical structure of precipitating clouds: the 27 July case

Figure 5 describes the atmospheric vertical structure and the precipitating clouds over the Hoggar on 27 July around midday, using radiosonde and CloudSat observations. The Tamanrasset sounding at 1200 UTC (Figure 5(a)) shows a residual Saharan atmospheric boundary layer (SABL) up to ∼5.6 km msl, which has

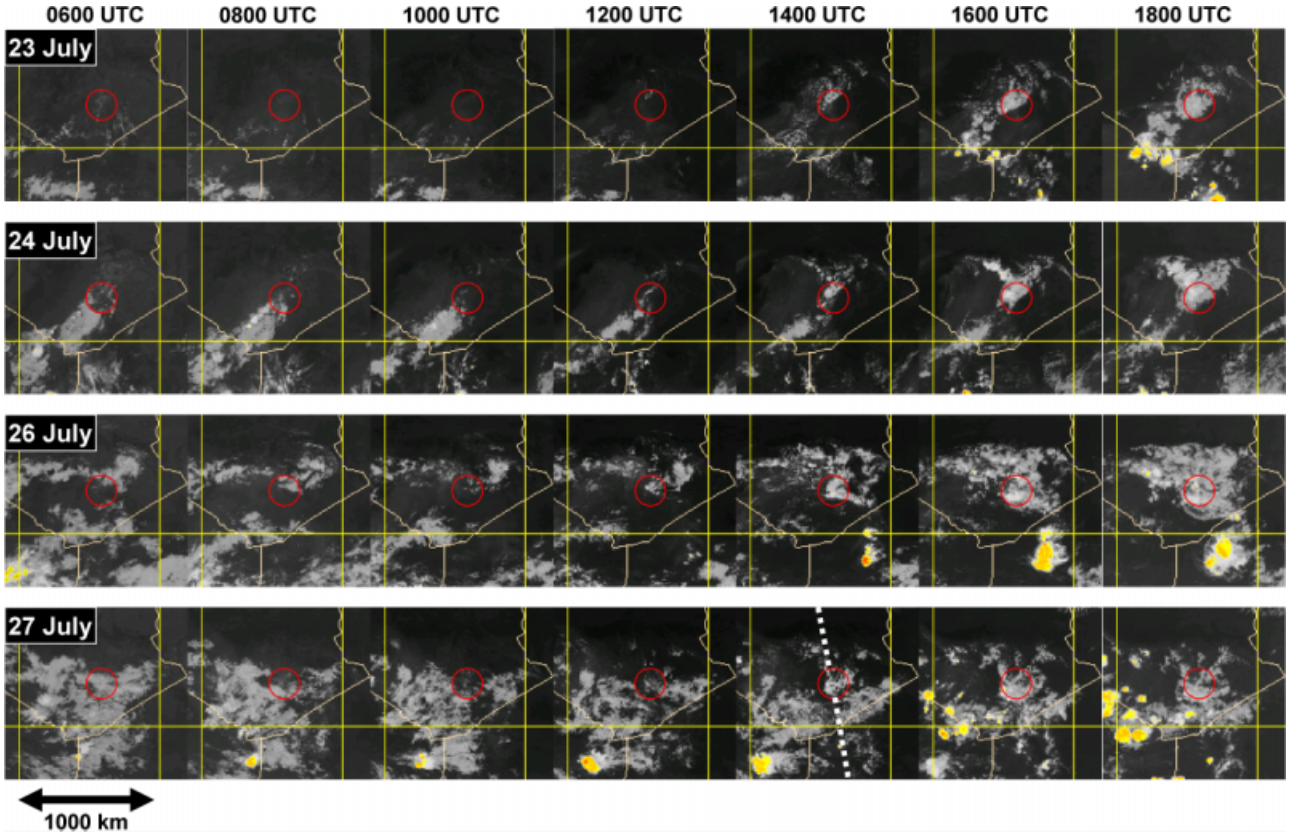

Figure 4. Diurnal evolution of cloud cover over the Hoggar (Tamanrasset in the dark grey (red) circle) and surrounding area from SEVIRI infrared (10.8 mum) with a white (yellow) colour threshold at −40°C. The dotted white line indicates the CloudSat orbit on 27 July. This figure is available in colour online at www.interscience.wiley.com/journal/qj

developed during the afternoon of the day before. Within the SABL, a moister (∼8 g kg^{-1}) CBL is developing up to ∼3.8 km msl. At 1200 UTC, the CBL top already reaches up to the LCL (at ∼3.7 km msl), thus leading to local cloud formation (as for the other three days of precipitation, see Table I). Note that at Tamanrasset the CBL may rapidly grow around midday at a rate of about 1 km per hour (Cuesta *et al*., 2008). At 1307 UTC (see Figure 5(b)), a cloud system is developing over the Hoggar up to ∼9 km msl (above the level of free convection (LFC) at ∼4.7 km), with a base around ∼3.8 km msl (i.e. the top of the CBL and ∼2.4 to 2.8 km agl). The CloudSat classification algorithm identifies these clouds as nimbostratus (Figure 5(b)), which are likely to produce steady moderate to heavy precipitation. As these clouds over the Hoggar have a higher cloud base than typical midlatitude nimbostratus (below 2 km agl, e.g. Houze, 1993), they are expected to be more convective. Beneath the clouds, liquid precipitation is observed and identified by CloudSat (see Figure 5(b)). This precipitation only reaches the ground after 1500 UTC (according to ground observations), being virga at first. The evaporation of virga is then likely to contribute to some extent to an increase in *RH* in the sub-cloud layer.

Higher humidity is likely to favour the formation of deeper clouds, by lowering the LCL and the LFC and thus facilitating the occurrence of deep convection. The top of these clouds may then be sufficiently cold (below −20°C) for ice crystal formation (e.g. Mason, 1971; Pruppacher and Klett, 1997). Such clouds are likely to grow even deeper since cold phase microphysical processes provide an additional buoyancy source as compared to warm phase processes alone (e.g. Houze, 1993). These conditions are likely to be reached on 27 July over the Hoggar (see Figure 5(b)) as the cloud-top temperature is below −25°C. The precipitation efficiency also increases due to the presence of ice crystals, capable of rapidly absorbing water vapour and forming bigger precipitation particles. These large hydrometeors are likely to: (1) fall faster than the ascending parcels while growing by aggregation and riming, (2) melt after crossing the 0°C level (typically 1–2 km below, e.g. Houze, 1993) to become rapidly falling raindrops that escape the cloud base, and (3) survive evaporation underneath the cloud to finally reach the ground (e.g. Mason, 1952; Houze, 1993). Moreover, as the air underneath the cloud base is more humid than usual, the hydrometeors travel longer distances before evaporation and the probability of reaching the ground is higher (Mason, 1952). This is consistent with Table II, which presents a comparison between a series of cases with precipitating and non-precipitating clouds over the Hoggar in 2006. In the absence of rain, the mean *RH* in the CBL is ∼36%, the cloud tops reach 7.4 km msl with a temperature <-19°C. In the case of precipitation, clouds form up to ∼10 km msl, consistent with an increase in

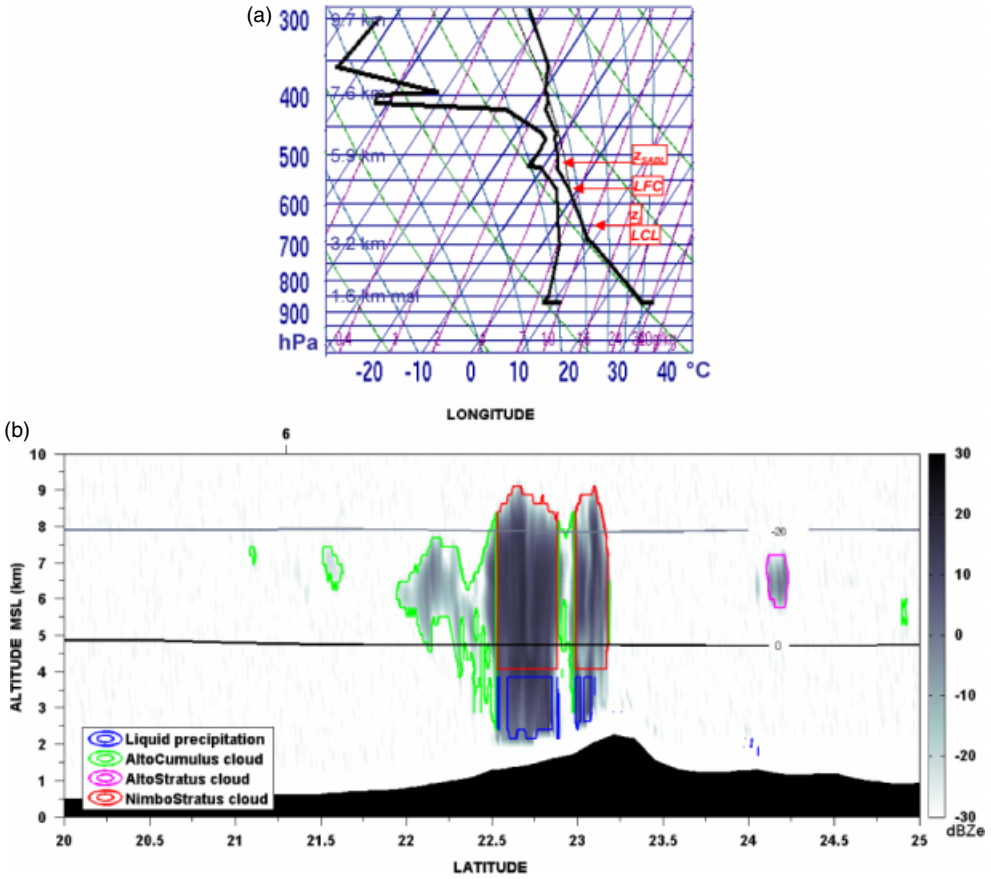

Figure 5. (a) Skew-*T* log-*p* diagram of Tamanrasset radiosounding on 27 July at 1200 UTC with q (left) and potential temperature θ (right). (b) CloudSat radar transect over West Africa on 27 July 2006 at 1307 UTC of reflectivity corrected for gas attenuation, with CloudSat level-2 classification in colour contours and ECMWF 0°C and −20°C isotherms. The separation between the liquid water and nimbostratus cloud classification is here done by estimating the cloud base at ∼3.7 km msl using the LCL obtained from the radiosounding. The outline of the topography appears in black. Ground echoes were removed. This figure is available in colour online at www.interscience.wiley.com/journal/qj

RH in the CBL up to ∼50% (up to ∼9.2 km msl with *RH* of ∼40% in the CBL, for the cases with precipitation occurring only at one site, see Table II). The cloud top reaches a temperature of −37°C, favourable for ice crystal formation. In all cases with (without) precipitation with the cloud top temperature below −20°C, the mean *RH* in the CBL is above (below) 35%. In most (∼80%) cases with rain, the cloud top temperature is below −20°C at about 1300 UTC (the time of CALIPSO overpass). The LCL in the rainy cases is lower than in the absence of rain (∼4.2 and ∼5.2 km msl, respectively), and we expect a lower cloud base in the cases with precipitation. In consequence, an increase in low-level moisture induces not only the formation of deeper clouds with possible ice formation (larger hydrometeors), but also lower cloud bases shortening the distance down to the ground, with less evaporation in the sub-cloud layer, thus more precipitation reaching the ground.

4. Large-scale conditions affecting the Hoggar during 21–28 July 2006

As mentioned in section 3, the two humidity peaks which lead to rainfall over the Hoggar during 21–28 July 2006 are associated with two northward bursts of the WAM reaching the massif. This period is characterized as well by cold-pool outflows and the strongest AEW event of the season reaching the Hoggar. Weaker AEW events with coincident precipitation, but in much lower quantity, were observed on five other occasions during the summer of 2006. During two of these events, cold-pool outflows reached the Hoggar Massif. With much drier conditions, no precipitation occurred as one AEW event and six cold pools reached the Hoggar in 2006 (see Cuesta *et al.*, 2008).

The following subsections describe the contributions from different components of the WAM (the SHL, the AEWs and the MCS cold pools) before (section 4.1) and during the first (section 4.2) and second (section 4.3) rainy events in the Hoggar during 21–28 July 2006.

4.1. Before the rainfall event in the Hoggar (20–22 July)

On 20 July, an MCS formed over central Niger (e.g. Barthe *et al.*, 2009). A trough of an AEW is located northeast of the MCS (the only case affecting the Hoggar during this period), thus probably increasing the atmospheric instability. The MCS generated a cold-pool outflow, which propagated northwards ∼900 km up to the

Table II. Characteristics of the cloud structure over the Hoggar as obtained from 25 daytime CALIPSO overpasses between 1 June and 31 October 2006.

Case type	**Cloud top** (km msl)	**Temp. at cloud top** (°C)	**CBL top** (km msl)	**LCL** (km msl)	***RH* in CBL** (°C)	***q* in the CBL** (g kg^{-1})	***RH* below LCL** (%)	***q* below LCL** (g kg^{-1})
Rain at both sites	10.0 (±2.2)	−37(±17)	4.7 (±1.3)	4.2 (±0.7)	50 (±8)	6.2 (±2.1)	46 (±11)	6.4 (±2.0)
Rain at one site	9.2 (±2.2)	−31(±14)	4.6 (±0.9)	4.5 (±0.3)	40 (±9)	5.3 (±0.8)	38 (±5)	5.3 (±0.8)
No rain	7.4 (±2.2)	−19(±16)	5.5 (±0.5)	5.2 (±0.5)	36 (±7)	3.8 (±1.0)	33 (±6)	3.9 (±1.2)

The related atmospheric vertical structure as derived from the 1200 UTC radiosondes in Tamanrasset is given. A classification is done using precipitation measurements in Tamanrasset and Assekrem during the same period. Cases are sorted out based on the fact that there is (1) rainfall in Tamanrasset and Assekrem (5 cases), (2) rainfall in only one of the sites (7 cases) or (3) no rainfall at all (13 cases). Mean quantities of each case type are displayed, with the standard deviation indicated by (±). Cloud top altitudes are derived from CALIPSO soundings over the Hoggar. Observations of temperature, LCL, *RH* and *q* were taken from Tamanrasset radiosondes.

Hoggar. On 21 July at about 2100 UTC (Figure 6(a)), the cold pool arrives at the Hoggar. At this time (between 21 and 22 July), no significant increase in humidity is observed in Tamanrasset (Figure 3(a)–(b)). On the other hand, observations in Tamanrasset and Assekrem show a reduction of the visibility accompanied by an increase in aerosol optical depth (AOD) or aerosol concentration at the surface (Figure 3(d)–(e)). Figure 6(a) shows a second cold pool emanating from an MCS passing in the vicinity of the Aïr Mountains. In the evening of 22 July, the two first dust plumes merge and move around the south-western boundaries of the Hoggar (Figure 6(b)). A third dust front starts propagating north ahead of an MCS near the Niger–Mali–Algeria frontier and approaches the forelands of the Hoggar (Figure 6(b)).

On 21 and 22 July, the ITD exhibits a northward prominence in the longitude band 0–5°E reaching the southwest forelands of the Hoggar (Figure 6(c) and (e)). The south-westerly winds along the south-eastern flank of the SHL are favouring the northward progression of the ITD in this region. The SHL is split into two cores, one in the vicinity of the Hoggar at ∼2°E and the other more to the west (Figure 6(c) and (e)). On both 21 and 22 July, strong north-easterly harmattan winds are observed across central Algeria and northern Mali at the north-eastern flank of the SHL (Figure 6(c) and (e)). Such winds may induce a reinforcement of the SHL cyclonic circulation, which is indicated by an increase in relative vorticity near 22°N 3°W by a factor of 2 to 4 with respect to the previous days (not shown).

Figure 6(d) and (f) show AEWs propagating westwards towards the Atlantic at a speed of ∼10 degrees longitude per day, with a periodicity of 3 days and a wavelength of ∼3000 km (as for some cases reported in Fink and Reiner (2003)). On 22 July, the northern part of an AEW south sector (shaded blue in Figure 6(d) and (f)) reaches the Hoggar, reinforcing the WAM southerly flow in this region. A wave trough at the northern Mali–Mauritania frontier possibly reinforces the western core of the SHL (see Figure 6(e)–(f)).

4.2. During the first rainfall event in the Hoggar (23–24 July)

On 23 July, the south sector of the AEW propagates to the southwest of the Hoggar and the south-westerly winds around a wave ridge at ∼18°N ∼8°E reinforce the advection towards the Hoggar (see Figure 7(d)). The western core of the SHL deepens and moves westwards (Figure 7(c)), with its circulation reinforcing the northward progression of the ITD. A wave trough at ∼20°N ∼17°W is located in the southern boundary of the SHL western core, possibly contributing to its deepening.

South of the Hoggar, the cold-pool outflows formed the day before merge together into a large dust front which advances northwards (see Figure 7(a)). The leading edge of the front reaches the ITD, presumably favouring its advance (as in Flamant *et al*., 2009), from a position to the southwest of the Hoggar at 0600 UTC (Figure 7(c)) until reaching the western Hoggar at 1030 UTC (Figure 7(a)). In Tamanrasset, humidity increases significantly (by ∼30% in *q*, see Figure 3(a) on 23 July) accompanied by an increase in AOD and a drop in visibility (see Figure 3(d)).

On 24 July, the ITD has advanced up to the western Hoggar (Figure 7(e)). The north sector of an AEW reaches the Hoggar and it starts advecting drier air from the northern Sahara (Figure 7(f)). The SHL eastern core weakens on 24 July (Figure 7(e)) and moves westwards on 25 July (Figure 7(g)). This is likely to be linked to the surface cooling in the vicinity of the Hoggar induced by the increase in cloud shading and rainfall on 23 and 24 July.

On 25 July, the ITD clearly withdraws west from the Hoggar (Figure 7(g)). At Tamanrasset, both humidity and dust load strongly drop (by >50% in *q* and AOD, see Figure 3(a) and (d)).

4.3. During the second rainfall event in the Hoggar (26–27 July)

During the afternoon of 25 July, two new cold-pool-associated dust plumes are formed along the Algeria–Niger frontier and advance northwards (Figure 8(a)).

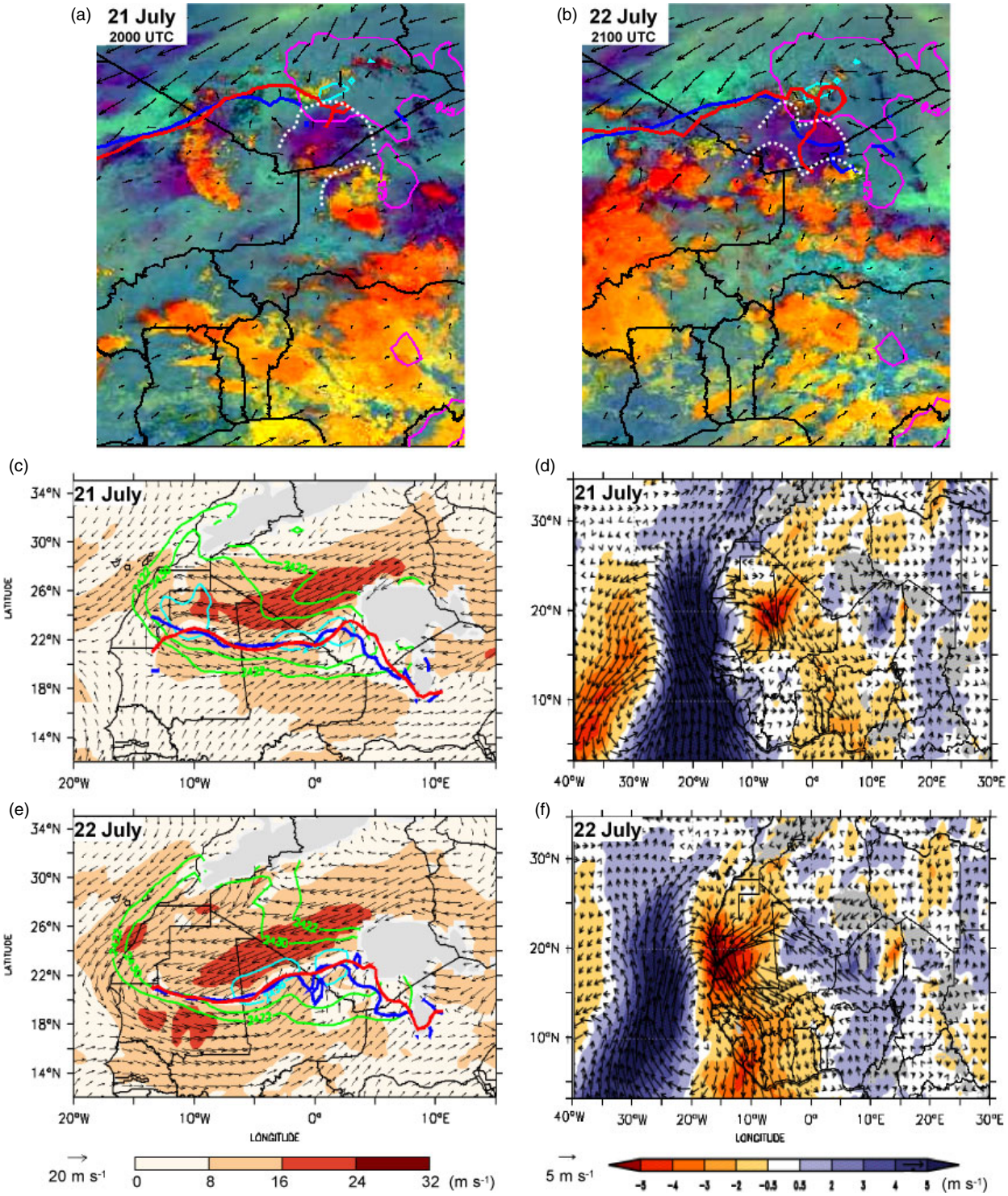

Figure 6. (a) SEVIRI-derived false colour images over West Africa (over and south of the Hoggar) on 21 July (at the time indicated), showing dust as proxy for cold pools (dark grey/purple-red), clouds (light grey/orange-yellow) and differences in surface emissivity retrieved in absence of dust or clouds (grey/green-magenta). Contours of the orography exceeding the 925 hPa (dark grey/pink) and 850 hPa (light grey/magenta) pressure levels are outlined. Dotted white lines indicate the leading edge of cold-pool-associated dust fronts approaching the Hoggar. The ITD position is indicated in dark grey (red) (1 m s^{-1} south-easterly wind at 10 m) and in black (blue) (minimum in geopotential at 925 hPa). (b) Same as (a) but for 22 July. (c) ECMWF analysis over West Africa at 0600 UTC on 21 July of (1) 925 hPa winds (arrows and shading), (2) the SHL location and depth depicted by geopotential height difference between 700 hPa and 925 hPa (contours of 2438 m in light grey/magenta and 2430 and 2422 m in grey/green) and (3) the ITD position as on (a). (d) African easterly waves activity on 21 July at 0600 UTC, described by ECMWF 850 hPa winds filtered between 3 and 5 days. South and north sectors are shaded in dark grey/blue and grey/orange, respectively. (e) and (f) Same as (c) and (d), respectively, but for 22 July. This figure is available in colour online at www.interscience.wiley.com/journal/qj

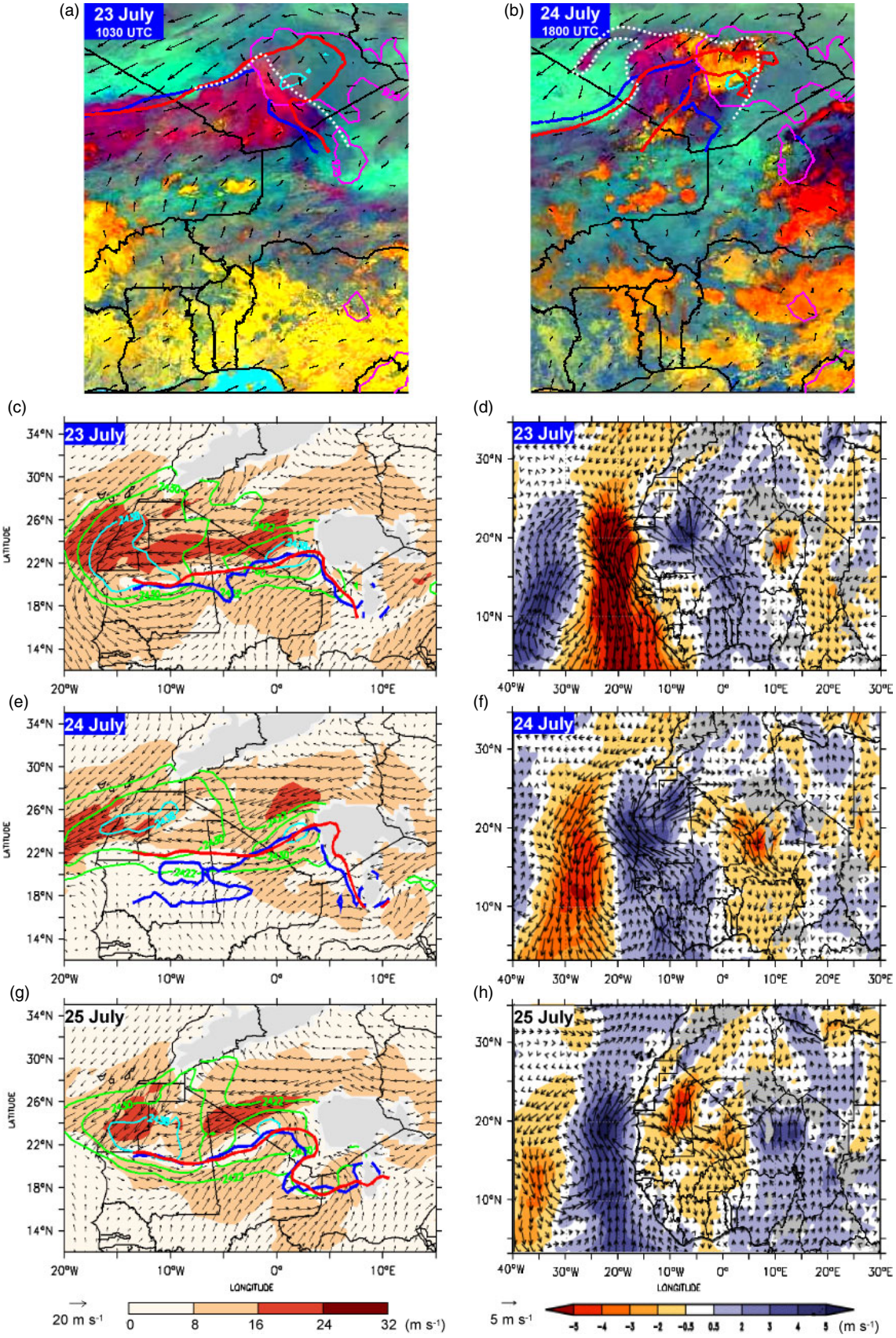

Figure 7. (a) and (b) Same as Figure 6(a) but for 23 July and 24 July, respectively. (c) and (d) Same as Figure 6(c) and (d), respectively, but for 23 July. (e) and (f) Same as Figure 6(c) and (d), respectively, but for 24 July. (g) and (h) Same as Figure 6(c) and (d), respectively, but for 25 July. This figure is available in colour online at www.interscience.wiley.com/journal/qj

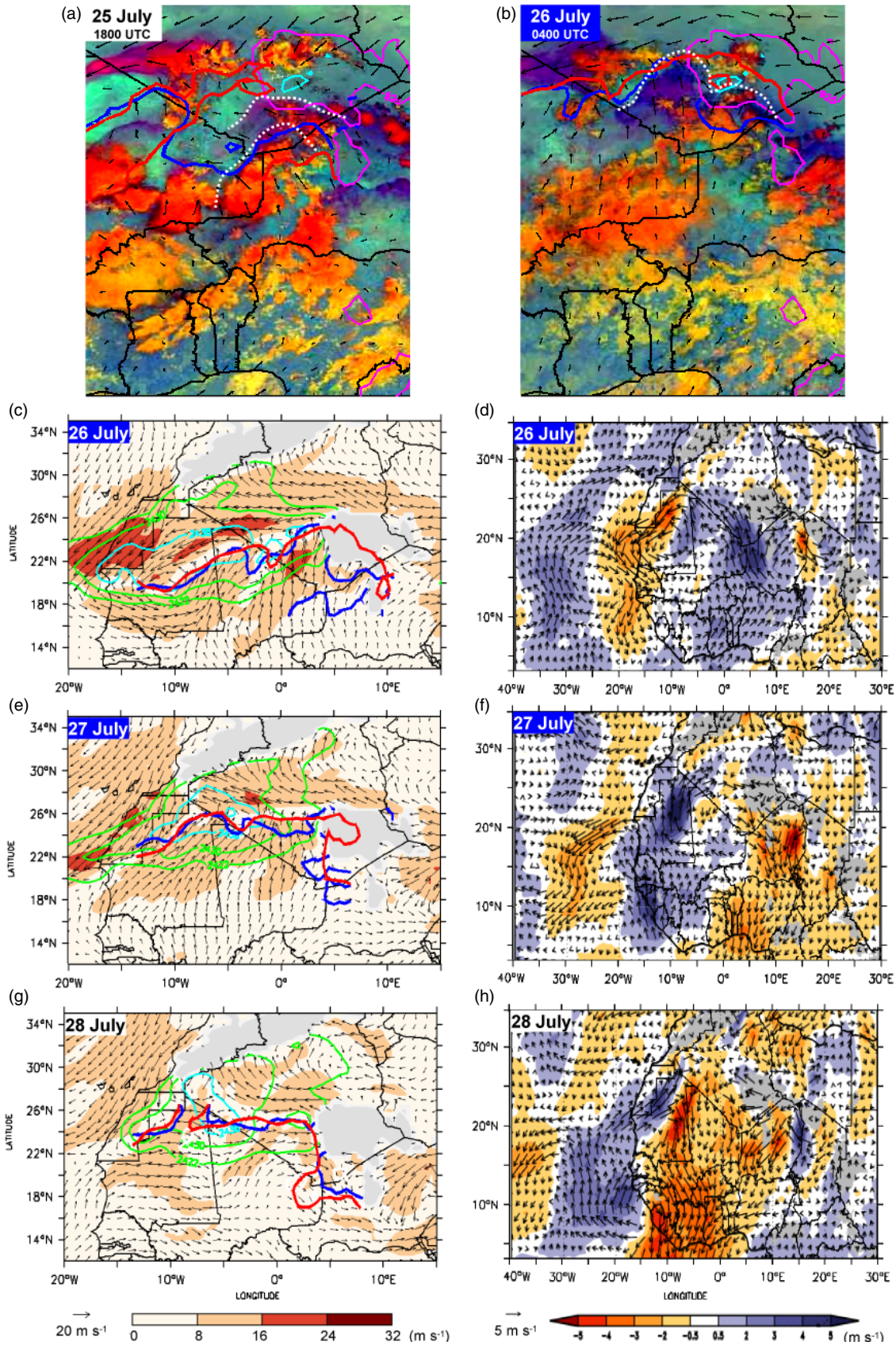

Figure 8. (a) and (b) Same as Figure 6(a) but for 25 July and 26 July, respectively. (c) and (d) Same as Figure 6(c) and (d), respectively, but for 26 July. (e) and (f) Same as Figure 6(c) and (d), respectively, but for 27 July. (g) and (h) Same as Figure 6(c) and (d), respectively, but for 28 July. This figure is available in colour online at www.interscience.wiley.com/journal/qj

At about 0400 UTC on 26 July (Figure 8(b)), cold-pool outflows merge together into a dust front that reaches the ITD. In addition, a new strong (>3 m s^{-1}) south sector of an AEW favours the southerly advection towards the western Hoggar (see Figure 8(d)). Again a wave trough (near ∼21°N ∼7°W) is located near a deeper SHL core (see Figure 8(c) and 8(d)). The winds along the south-eastern flank of the SHL favour the WAM southerly flow. As a result of the various contributions, the monsoon flow strongly intensifies near 22°N 1°E (>18 m s^{-1} at 925 hPa, see Figure 8(c)) and reaches the Hoggar, advancing until ∼9°W. The arrival of the ITD contributes once again to a coincident increase in humidity and decrease in visibility in Tamanrasset and Assekrem (see Figure 3(a), (d) and (e)).

On 27 July the ITD advances, advecting humidity further north (from 5°E to 10°W, Figure 8(e)). The SHL weakens, with a main core west of 4°W (Figure 8(e)), and a new north sector of an AEW reaches the Hoggar (Figure 8(f)). On the following day (28 July), this north sector causes the southward advection of drier air between the Hoggar and ∼10°W (Figure 8(h)), in concomitance with the withdrawal of the ITD (Figure 8(g)) and the end of the rainfall event.

To sum up, during both rainy events favourable large-scale conditions consistently add up until the ITD reaches the Hoggar. One day before and during the WAM northward burst, the monsoon flow is strengthened by both a south sector of an AEW and the south-westerly winds along the south-eastern flank of the SHL (see Table III). With the additional contribution of cold-pool outflows merging with the ITD and pushing it northwards, the WAM surges reach the Hoggar (Table III). Two days after, the ITD retreats with the occurrence of an AEW north sector, and the rainfall events end (Table III).

5. Climatology of WAM-associated rainfall in the Hoggar

Most precipitation in the Hoggar, both in terms of number of events and amount, occur during the summer season (i.e. from June to September, Figure 9). Some influence of midlatitude troughs is expected at the end of May and beginning of June, as reported by Knippertz (2008). The WAM is more likely to directly affect the southern Sahara during its mature phase when the ITD exhibits its northernmost position. This period starts with the monsoon onset, which corresponds to the beginning of the rainy season in the Sahel, typically around 24 June, with a variability of ±8 days (Sultan and Janicot, 2000, 2003). It lasts until the middle of September, when the intertropical convergence zone (ITCZ) retreats southward, and the rainy season in the Sahel comes to an end. The case of 23–27 July 2006 (described in sections 3 and 4) occurs in the mature monsoon phase, shortly after an atypically late monsoon onset (between 17 and 21 July, see Janicot and Sultan, 2007) due to enhanced subsidence over the whole of West Africa.

We focus on the peak monsoon period from 1 July to 15 September of the ERA-40 1979–2001 epoch to analyse the wind and geopotential fields. We consider all the days with precipitation measured by ONM in excess of 0.1 mm simultaneously in Tamanrasset and in Assekrem (106 cases). Then, composites over each 'precipitation day' (D) at 0600 UTC, as well as the four days before and after

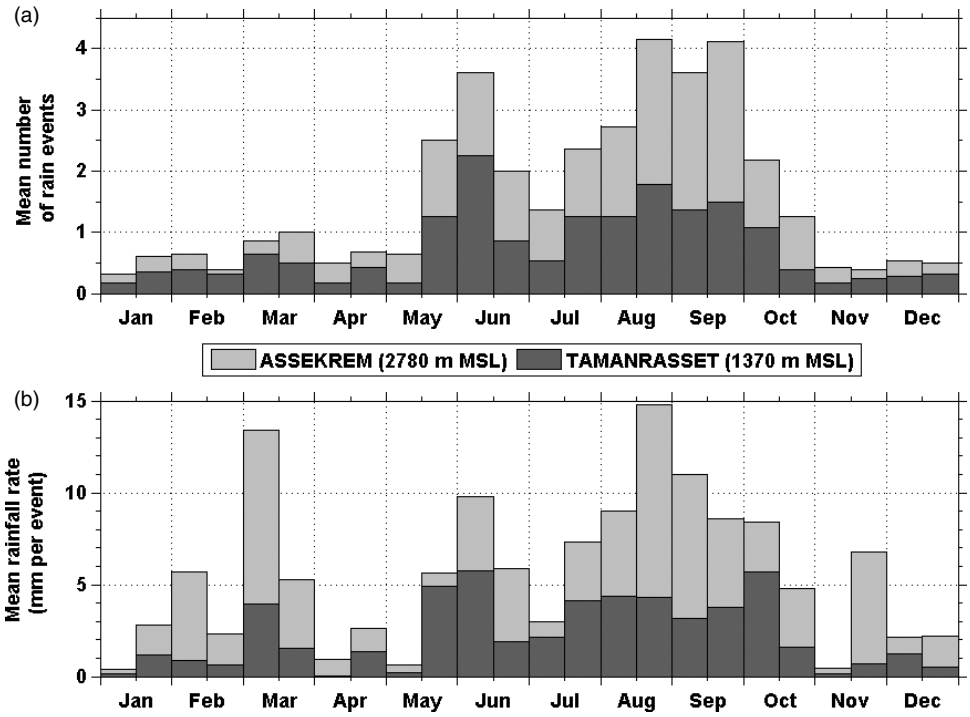

Figure 9. Mean annual evolution of precipitation in Tamanrasset and Assekrem from 1979 to 2006. (a) Number of rainy days, 1st to 15th and 16th to the end of each month. (b) Rainfall amount per rain event.

the rain event in the Hoggar, are constructed. Composited fields are the occurrence and mean location of AEWs (Figure 10) as well as the mean position of the SHL and the ITD (Figure 11). Figure 10 shows the occurrence of AEWs around the day of precipitation over the Hoggar, which on average propagate ~6.5 degrees longitude per day, with a periodicity of 4 days and a wavelength of approximately 2500 km. Confirming the results from the case-study (section 4), the precipitation day is preceded (on D−1 and D) by the passage of a strong south sector of an AEW that enhances the advection of moist monsoonal air towards the Hoggar. Two days before (D−2) and two days after (D+2), a northerly wave sector is located in the southwest boundaries of the Hoggar, contributing to a withdrawal of the WAM moist air. Similar results are obtained when considering only cases with precipitation above 0.8 mm (44 cases) and 1 mm (38 cases) (not shown).

Figure 11 shows the progression of the ITD from a position southwest of the Hoggar on D−3 to the forelands of the Hoggar on D−1. Finally, the ITD reaches the Hoggar on the day when precipitation occurs. On D+2, the ITD withdraws southward progressively and the day after (D+3, not shown) it retreats to a position southwest of the Hoggar (as on D−3). The SHL depth and location show a coherent day-to-day evolution, which is probably linked to the impact of the northern excursion of the ITD. Before the northward advance of the ITD (D−3 and D−2), a deep SHL core extends from 10°W to 2°E between 25 and 30°N. As the ITD shifts north, increasing cloud shading and precipitation, the SHL weakens and becomes shallower (from D to D+2). On D+2, a weak SHL core is located on the western forelands of the Hoggar (from 5°W to 5°E and 22° to 26°N), with a cyclonic circulation no longer contributing to advection towards the Hoggar.

6. Summary and conclusions

The present paper shows that summer precipitation over the Hoggar is triggered by the increase in humidity often associated with the WAM. Low-level moisture is the dominating limiting factor for rainfall over the massif. As it is increased, the cloud tops are higher, with possible ice formation (larger hydrometeors), the cloud bases are lower and less evaporation occurs in the sub-cloud layer. As the WAM reaches the Hoggar, the *RH* in the CBL exceeds ~45% and precipitation reaches the ground (otherwise, virga are observed).

The northward bursts of a mature monsoon, from a position around 20/21°N up to the Hoggar, are directly linked to the occurrence of AEWs, MCS-associated cold pools and a favourable SHL cyclonic circulation. The northward advance of the ITD is reinforced by a south sector of an AEW at the southwest forelands of the

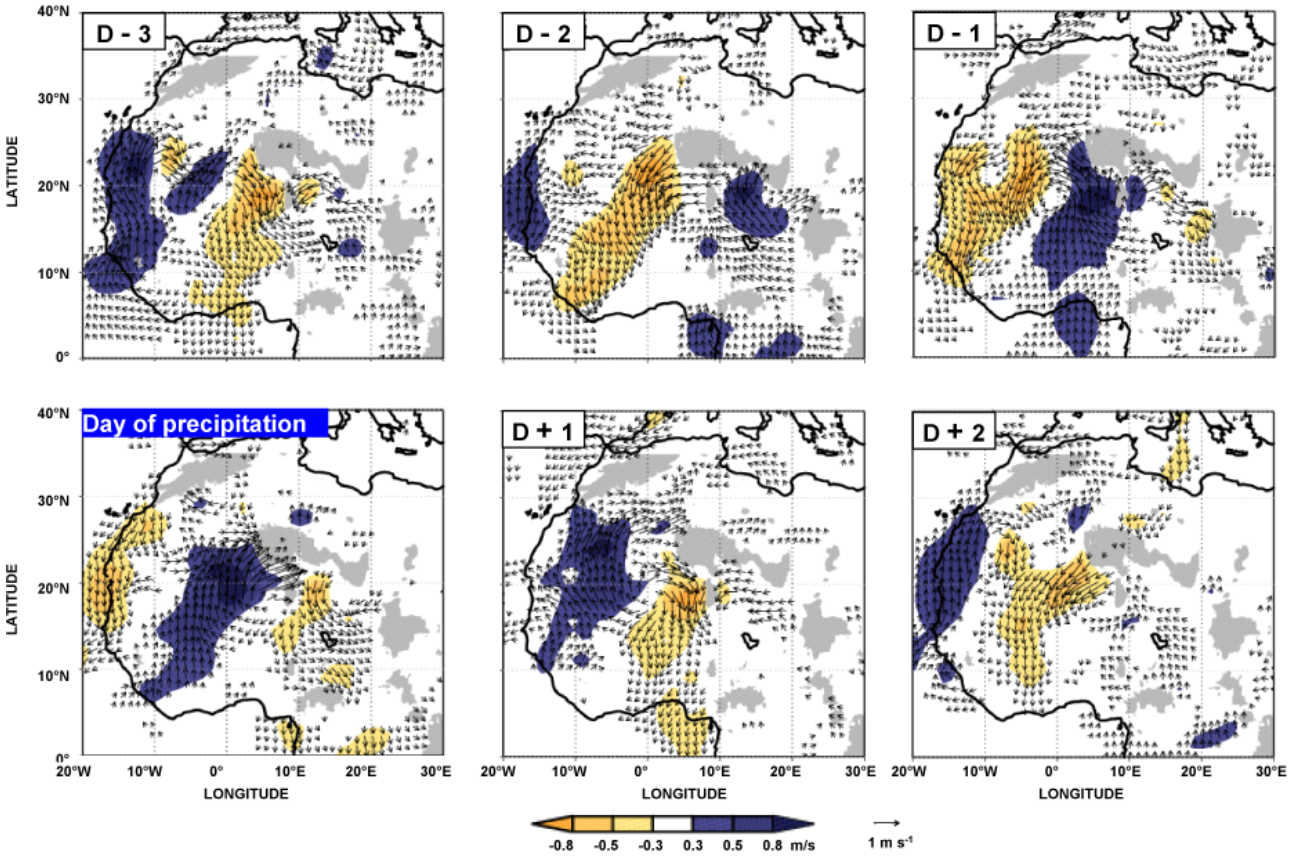

Figure 10. Composite of the mean AEW activity (850 hPa 3–5-day filtered winds at 0600 UTC) from three days before (D−3) to two days after (D+2) the 'day of precipitation D' over the Hoggar (both in Tamanrasset and Assekrem) from 1 July to 15 September (using ERA-40 re-analysis between 1979 and 2001). This figure is available in colour online at www.interscience.wiley.com/journal/qj

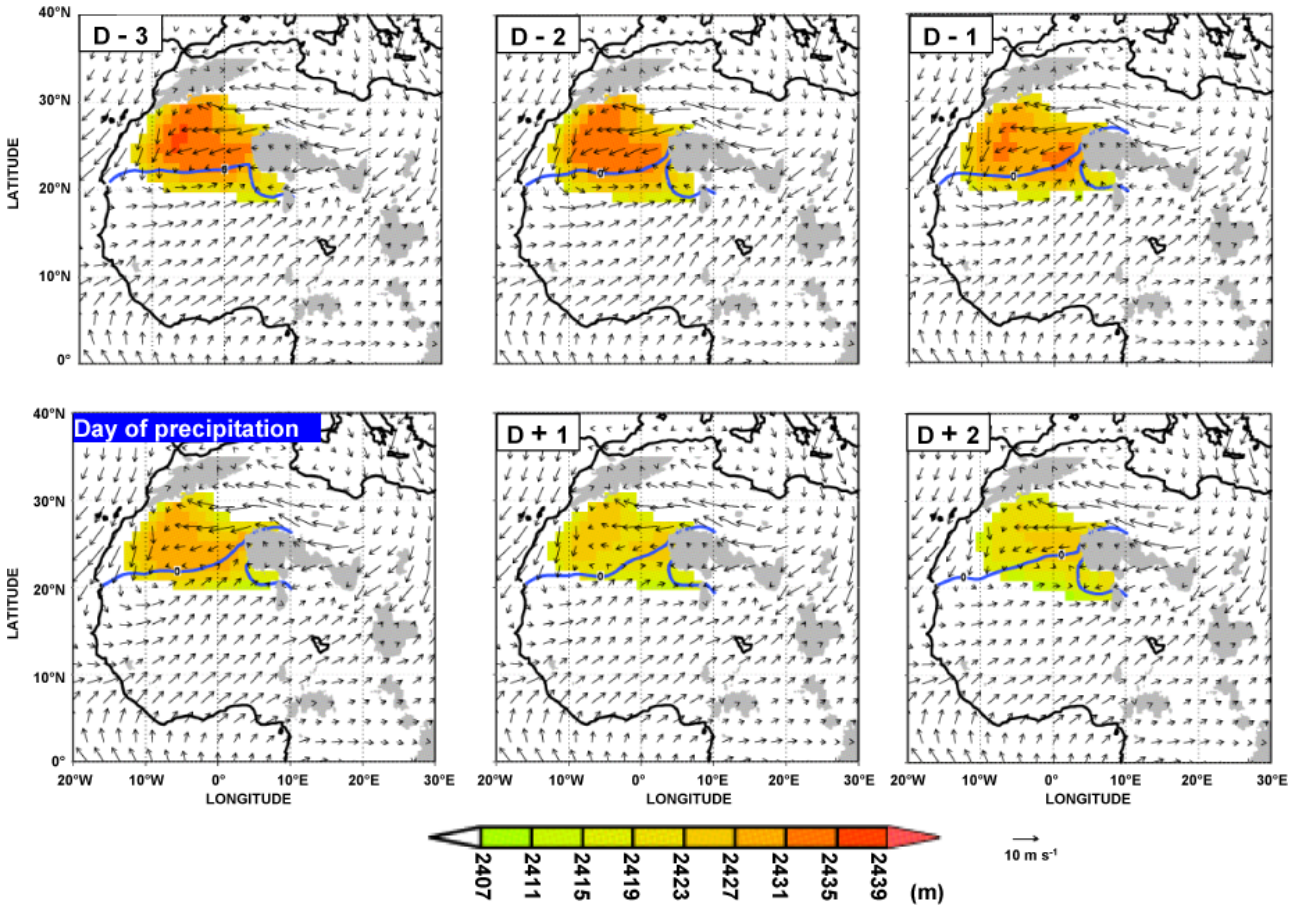

Figure 11. Same as Figure 10 for the SHL depth (shade) shown by geopotential height difference between 700 hPa and 925 hPa and ITD location (dark grey/blue line) depicted by the minimum geopotential gradient at 925 hPa. This figure is available in colour online at www.interscience.wiley.com/journal/qj

Hoggar and by the south-westerly winds along the south-eastern flank of the SHL. The WAM is seen to reach the Hoggar when cold-pool outflows originating over Niger merge with the ITD, favouring its northward advance.

These results are mainly representative for the Hoggar massif region, covering an extent of approximately 400 000 km^2. Similar conditions might be expected in other mountainous regions of the southern Sahara such as the Tibesti massif. The orography of the Hoggar plays a significant role for the low-level atmospheric circulation (on the WAM progression and the SHL cyclonic circulation, see section 1) as well as for the triggering of deep convection clouds over the Sahara (see section 2). Deep convection anvils originating over these mountains are likely to affect the regional climate and precipitation distribution.

Further analyses are needed to determine the capability of numerical models to forecast the WAM northward surges and subsequent precipitation over populated regions in the southern Sahara such as the Hoggar Massif. ECMWF forecast of precipitation over the Sahel has shown an improvement in presence of AEWs and strong convective activity (i.e. Söhne *et al*., 2008). Further investigation is required to establish if a similar impact is expected for precipitation over the Hoggar. Due to the lack of observations in this region, particular attention should be given to the impact of low-level moisture on cloud microphysics and droplet evaporation.

Acknowledgements

'Based on a French initiative, AMMA was built by an international scientific group and is currently funded by a large number of agencies, especially from France, UK, US and Africa. It has been the beneficiary of a major financial contribution from the European Community's Sixth Framework Research Programme. See http://www.amma-international.org'. We thank John Marsham and Gerry Devine from the University of Leeds and Jacques Pelon from LATMOS for fruitful discussion regarding cold pools and precipitating clouds. The authors would like to thank K. Ramage and S. Cloché (Institut Pierre Simon Laplace, France) for facilitating access to ECMWF and CALIPSO data, as well as L. Gonzalez and C. Deroo (Laboratoire d'Optique Atmosphérique) for supplying the SEVIRI composite images. We are grateful to the Centre National d'Études Spatiales (CNES), and the NASA Langley ASDC User Services, Cloud-Aerosols-Water-Radiation Interactions (ICARE) and CIRA CloudSat data-processing data centres for supplying the CALIPSO and CloudSat data. The authors acknowledge the AERONET/PHOTONS

Table III. Influence of the AEW, SHL and cold-pools favouring (+) or impeding (or not favouring) (−) the northward progression of the ITD, which brings humidity over the Hoggar.

Date	AEW	SHL	Cold pools	Total	ITD
21 July	Weak northerly flow (−)	Acceleration of the SHL cyclonic circulation (+)	A cold pool arrives but without increase in humidity in the Hoggar (+)	++−	Southwest of Hoggar
22 July	Southeasterly flow over the Hoggar by an AEW south sector (+)	Acceleration of the SHL cyclonic circulation (+)	No cold pools over the Hoggar (−)	++−	Southwest of Hoggar
23 July	Southwesterly flow over western Hoggar by an AEW south sector (++)	Partial westward displacement, with a deep western core and a remaining eastern core (+)	A cold pool merges with the ITD and humidity increases (++)	+++++	Arrival around 1030 UTC
24 July	Weak northerly flow (−)	Weakening of the western core and a remaining eastern core (−)	A cold pool is generated over the Hoggar and propagates westwards (−)	−−−	Continuance over western Hoggar
25 July	Southerly flow over southern Hoggar by an AEW south sector (+)	Westward displacement of the eastern core and deepening of the western core (+)	No cold pools over the Hoggar (−)	++−	Withdrawal
26 July	Strong southwesterly flow over western Hoggar by an AEW south sector (++)	Westward merging of the eastern core into a single SHL core, with maximum depth in Mauritania (++)	A cold pool merges with the ITD and humidity increases (++)	++++++	Arrival around 0400 UTC and advance over the Hoggar
27 July	Weak northerly flow (−)	Continuance in the western location and weakens (−)	A cold pool is generated over the Hoggar and propagates westwards (−)	−−−	Continuance over western Hoggar
28 July	Strong northerly flow (−)	Continuance in the western location and weakens (−)	No cold pools over the Hoggar (−)	−−−	Withdrawal

A clear positive influence or the superposition of two conditions is indicated by (++). The dates of precipitation are shaded in dark grey. All positive conditions and the presence of the ITD over the Hoggar are shaded in light grey.

(P. Goloub from Laboratoire d'Optique Atmosphérique) for support on sun photometer operation in Tamanrasset.

References

Barthe C, Asencio N, Lafore J-P, Chong M, Campistron B. 2009. Multi-scale analysis of the 25–27 July 2006 convective period over Niamey: Comparison between Doppler radar observations and cloud-resolving simulations. *Q. J. R. Meteorol. Soc.* **136**(s1): 191–209.

Bock O, Bouin MN, Doerflinger E, Collard P, Masson F, Meynadier R, Nahmani S, Koité M, Gaptia Lawan Balawan K, Didé F, Ouedraogo D, Pokperlaar S, Ngamini J-B, Lafore J-P, Janicot S, Guichard F, Nuret M. 2008. West African Monsoon observed with ground-based GPS receivers during African Monsoon Multidisciplinary Analysis (AMMA). *J. Geophys. Res.* **113**: D21105, DOI:10.1029/2008JD010327.

Couvreux F, Guichard F, Bock O, Lafore J-P, Redelsperger JL. 2009. Monsoon flux pulsations over West Africa prior to the monsoon onset. *Q. J. R. Meteorol. Soc.* **136**(s1): 160–174.

Cuesta J, Edouart D, Mimouni M, Flamant PH, Loth C, Gibert F, Marnas F, Bouklila A, Kharef M, Ouchène B, Kadi M, Flamant C. 2008. Multiplatform observations of the seasonal evolution of the Saharan atmospheric boundary layer in Tamanrasset, Algeria, in the framework of the African Monsoon Multidisciplinary Analysis field campaign conducted in 2006. *J. Geophys. Res.* **113**: D00C07, DOI:10.1029/2007JD009417.

Dubief J. 1963. *Le climat du Sahara. Tome II: Les précipitations*. Université d'Alger, Institut de Recherches Sahariennes (in French).

Dubief J. 1979. Review of the North African climate with particular emphasis on the production of eolian dust in the Sahel zone and in the Sahara. Pp 27–48 in *Saharan dust: Mobilization, transport, deposition*, Morales C (ed). John Wiley and Sons.

Fink AH, Reiner A. 2003. Spatiotemporal variability of the relation between African Easterly Waves and West African squall lines in 1998 and 1999. *J. Geophys. Res.* **108**: 4332, DOI:10.1029/2002JD002816.

Flamant C, Chaboureau J-P, Parker DJ, Taylor CM, Cammas J-P, Bock O, Timouk F, Pelon J. 2007. Airborne observations of the impact of a convective system on the planetary boundary layer thermodynamics and aerosol distribution in the inter-tropical discontinuity region of the West African Monsoon. *Q. J. R. Meteorol. Soc.* **133**: 1175–1189.

Flamant C, Knippertz P, Parker DJ, Chaboureau J-P, Lavaysse C, Agusti-Panareda A, Kergoat L. 2009. The impact of a mesoscale convective system cold pool on the northward propagation of the intertropical discontinuity over West Africa. *Q. J. R. Meteorol. Soc.* **135**: 139–159.

Guichard F, Kergoat L, Mougin E, Timouk F, Baup F, Hiernaux P, Lavenu F. 2009. Surface thermodynamics and radiative budget in the Sahelian Gourma: Seasonal and diurnal cycles. *J. Hydrol.*, DOI:10.1016/j.jhydrol.2008.09.007, in press.

Heffter JL. 1980. 'Air Resources Laboratories Atmospheric Transport And Dispersion model (ARL-ATAD)'. NOAA Technical Memorandum ERL-ARL-81, 24 pp.

Houze Jr RA. 1993. *Cloud dynamics*. Academic Press.

Janicot S, Sultan B. 2007. 'The large-scale context on the West African Monsoon in 2006'. Pp 11–17 in Exchanges, Newsletter of the Climate Variability and Predictability Programme (CLIVAR), No. 41, Vol. 12 No. 2. Available at http://eprints.soton.ac.uk/45355/01/Exchanges_41.pdf.

Kållberg P, Berrisford P, Hoskins B, Simmons A, Uppala S, Lamy-Thépaut S, Hine R. 2005. 'ERA-40 atlas'. Technical report, ERA-40 Project Report Series No. 19, ECMWF, Shinfield Park, Reading, UK, 191 pp.

Knippertz P. 2008. Dust emissions in the West African heat trough – the role of the diurnal cycle and of extratropical disturbances. *Meteorologische Zeitschrift* **17**: 553–563.

Knippertz P, Deutscher C, Kandler K, Müller T, Schulz O, Schütz L. 2007. Dust mobilization due to density currents in the Atlas region: Observations from the Saharan Mineral Dust Experiment 2006 field campaign. *J. Geophys. Res.* **112**: D21109, DOI:10.1029/2007JD008774.

Knippertz P, Ansmann A, Althausen D, Müller D, Tesche M, Bierwirth E, Dinter T, Müller T, Von Hoyningen-Huene W, Schepanski K, Wendisch M, Heinold B, Kandler K, Petzold A, Schütz L, Tegen I. 2009. Dust mobilization and transport in the northern Sahara during SAMUM 2006: A meteorological overview. *Tellus B* **61**: 12–31.

Lafore J-P, Chapelet P, Mumba Z, Chapelon N, Dufresne M-C, Agbabu R, Abdoul-Aziz A, Hamidou H, Asencio N, Couvreux F, Nuret M, Garba A. 2007. 'Forecaster's guide for West African Synthetic Analysis/Forecast WASA/F'. Available from https://www.amma-eu.org/sections/work_packages/process-studies/wp2_1/deliverables/forecaster-s-guide-for.

Lavaysse C, Flamant C, Janicot S, Knippertz P. 2009a. Dynamics and impacts on convection of the intra-seasonal variabilities of the West African Heat Low. *Q. J. R. Meteorol. Soc.* **136**(s1): 142–159.

Lavaysse C, Flamant C, Janicot S, Parker DJ, Lafore J-P, Sultan B, Pelon J. 2009b. Seasonal evolution of the West African heat low: A climatological perspective. *Clim. Dyn.*, in press.

Lebel T, Parker DJ, Flamant C, Bourles B, Marticorena B, Mougin E, Peugeot C, Diedhiou A, Haywood JM, Ngamini JB, Polcher J, Redelsperger J-L, Thorncroft CD. 2009. The AMMA field campaigns: Multiscale and multidisciplinary observations in the West African region. *Q. J. R. Meteorol. Soc.* **135**: AMMA special edition.

Marsham JH, Parker DJ, Grams CM, Taylor CM, Haywood JM. 2008. Uplift of Saharan dust south of the intertropical discontinuity. *J. Geophys. Res.* **113**: D21102, DOI:10.1029/2008JD009844.

Mason BJ. 1952. Production of rain and drizzle by coalescence in stratiform clouds. *Q. J. R. Meteorol. Soc.* **78**: 377–386.

Mason BJ. 1971. *The physics of clouds*. Clarendon Press: Oxford.

Miller SD, Kuciauskas AP, Liu M, Ji Q, Reid JS, Breed DW, Walker AL, Mandoos AA. 2008. Haboob dust storms of the southern Arabian Peninsula. *J. Geophys. Res.* **113**: D01202, DOI:10.1029/2007JD008550.

Parker DJ, Burton RR, Diongue-Niang A, Ellis RJ, Felton M, Taylor CM, Thorncroft CD, Bessemoulin P, Tompkins AM. 2005. The diurnal cycle of the West African monsoon circulation. *Q. J. R. Meteorol. Soc.* **131**: 2839–2860.

Pruppacher HR, Klett JD. 1997. *Microphysics of clouds and precipitation.* Kluwer Acad.: Norwell, Mass.

Redelsperger J-L, Thorncroft CD, Diedhiou A, Lebel T, Parker DJ, Polcher J. 2006. African Monsoon Multidisciplinary Analysis: An international research project and field campaign. *Bull. Am. Meteorol. Soc.* **87**: 1739–1746.

Söhne N, Chaboureau J-P, Guichard F. 2008. Verification of cloud cover forecast with satellite observations over West Africa. *Mon. Weather Rev.* **136**: 4421–4434.

Sultan B, Janicot S. 2000. Abrupt shift of the ITCZ over West Africa and intra-seasonal variability. *Geophys. Res. Lett.* **27**: 3353–3356.

Sultan B. Janicot S. 2003. The West African monsoon dynamics. Part II: The 'preonset' and 'onset' of the summer monsoon. *J. Climate* **16**: 3407–3427.

Stephens GL, Vane DG, Boain RJ, Mace GG, Sassen K, Wang Z, Illingworth AJ, O'Connor EJ, Rossow WB, Durden SL, Miller SD, Austin RT, Benedetti A, Mitrescu C. 2002. The CloudSat mission and the A-Train. *Bull. Am. Meteorol. Soc.* **83**: 1771–1790.

Winker DM, Hunt WH, McGill MJ. 2007. Initial performance assessment of CALIOP. *Geophys. Res. Lett.* **34**: L19803, DOI:10.1029/2007GL030135.

